

## Supporting Material for

### Target Atmospheric CO<sub>2</sub>: Where Should Humanity Aim?

James Hansen,<sup>1,2\*</sup> Makiko Sato,<sup>1,2</sup> Pushker Kharecha,<sup>1,2</sup> David Beerling,<sup>3</sup>  
Valerie Masson-Delmotte,<sup>4</sup> Mark Pagani,<sup>5</sup> Maureen Raymo,<sup>6</sup> Dana L. Royer,<sup>7</sup> James C. Zachos<sup>8</sup>

**Paleoclimate data show that climate sensitivity is ~3°C for doubled CO<sub>2</sub>, including only fast feedback processes. Equilibrium sensitivity, including slower surface albedo feedbacks, is ~6°C for doubled CO<sub>2</sub> for the range of climate states between glacial conditions and ice-free Antarctica. Decreasing CO<sub>2</sub> was the main cause of a cooling trend that began 50 million years ago, large scale glaciation occurring when CO<sub>2</sub> fell to 425±75 ppm, a level that will be exceeded within decades, barring prompt policy changes. If humanity wishes to preserve a planet similar to that on which civilization developed and to which life on Earth is adapted, paleoclimate evidence and ongoing climate change suggest that CO<sub>2</sub> will need to be reduced from its current 385 ppm to at most 350 ppm. The largest uncertainty in the target arises from possible changes of non-CO<sub>2</sub> forcings. An initial 350 ppm CO<sub>2</sub> target may be achievable by phasing out coal use except where CO<sub>2</sub> is captured and adopting agricultural and forestry practices that sequester carbon. If the present overshoot of this target CO<sub>2</sub> is not brief, there is a possibility of seeding irreversible catastrophic effects.**

---

<sup>1</sup>NASA/Goddard Institute for Space Studies, New York, NY 10025, USA. <sup>2</sup>Columbia University Earth Institute, New York, NY 10027, USA. <sup>3</sup>Dept. Animal and Plant Sciences, University of Sheffield, Sheffield S10 2TN, UK. <sup>4</sup>Lab. des Sciences du Climat et l'Environnement/Institut Pierre Simon Laplace, CEA-CNRS-Universite de Versailles Saint-Quentin en Yvelines, CE Saclay, 91191, Gif-sur-Yvette, France. <sup>5</sup>Dept. Geology and Geophysics, Yale University, New Haven, CT 06520-8109, USA. <sup>6</sup>Dept. Earth Sciences, Boston University, Boston, MA 02215, USA. <sup>7</sup>Dept. Earth and Environmental Sciences, Wesleyan University, Middletown, CT 06459-0139, USA. <sup>8</sup>Earth & Planetary Sciences Dept., University of California, Santa Cruz, Santa Cruz, CA 95064, USA.

\*To whom correspondence should be addressed. E-mail: [jhansen@giss.nasa.gov](mailto:jhansen@giss.nasa.gov)

## Supporting Online Material

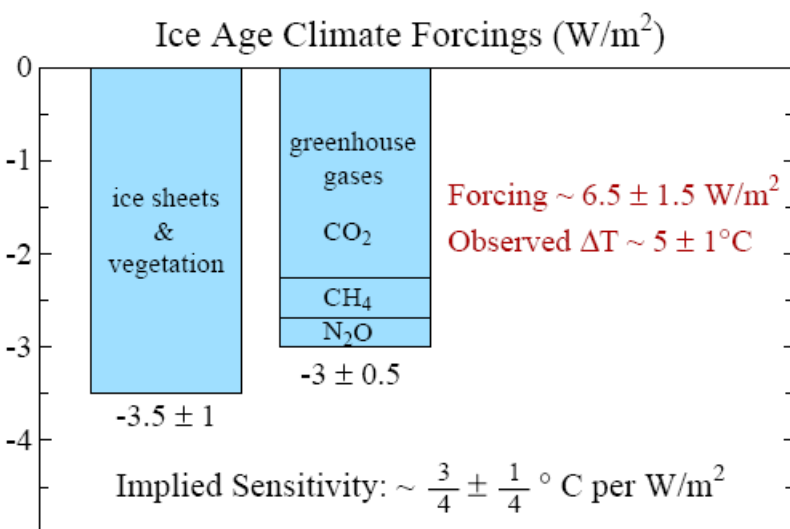


**Fig. S1. Climate forcings during ice age 20 ky BP, relative to the present (pre-industrial) interglacial period.**

**Ice age climate forcings.** Figure S1 shows the climate forcings during the depth of the last ice age, 20 ky BP, relative to the Holocene (13). The largest contribution to the uncertainty in the calculated  $3.5 \text{ W/m}^2$  forcing due to surface changes (ice sheet area, vegetation distribution, shoreline movements) is due to uncertainty in the ice sheet sizes (13, S1). Formulae (18) for the GHG forcings yield  $2.25 \text{ W/m}^2$  for  $\text{CO}_2$  (185 ppm  $\rightarrow$  275 ppm),  $0.43 \text{ W/m}^2$  for  $\text{CH}_4$  (350  $\rightarrow$  675 ppb) and  $0.32 \text{ W/m}^2$  for  $\text{N}_2\text{O}$  (200  $\rightarrow$  270 ppb). The  $\text{CH}_4$  forcing includes a factor 1.4 to account for indirect effects of  $\text{CH}_4$  on tropospheric ozone and stratospheric water vapor (11).

The climate sensitivity inferred from the ice age climate change ( $\sim 3/4^\circ\text{C per W/m}^2$ ) includes only fast feedbacks, such as water vapor, clouds, aerosols (including dust) and sea ice. Ice sheet size and greenhouse gas amounts are specified boundary conditions in this derivation of the fast-feedback climate sensitivity.

It is permissible to, alternatively, specify aerosol changes as part of the forcing and thus derive a climate sensitivity that excludes the effect of aerosol feedbacks. That approach was used in the initial empirical derivation of climate sensitivity from Pleistocene climate change (13). The difficulty with that approach is that, unlike long-lived GHGs, aerosols are distributed heterogeneously, so it is difficult to specify aerosol changes accurately. Also the forcing is a sensitive function of aerosol single scatter albedo, which is also not well measured, and the vertical distribution of aerosols in the atmosphere. Further, the aerosol indirect effect on clouds also depends upon all of these poorly known aerosol properties.

One recent study (S2) specified an arbitrary glacial-interglacial aerosol forcing slightly larger than the GHG glacial-interglacial forcing. As a result, because temperature, GHGs, and aerosol amount, overall, are positively correlated in glacial-interglacial changes, this study inferred a climate sensitivity of only  $\sim 2^\circ\text{C}$  for doubled  $\text{CO}_2$ . This study used the correlation of aerosol and temperature in the Vostok ice core at two specific times to infer an aerosol forcing for a given aerosol amount. The conclusions of the study are immediately falsified by considering the full Vostok aerosol record (Fig. 2, 16), which reveals numerous large aerosol fluctuations without any corresponding temperature change. In contrast, the role of GHGs in climate change is confirmed when this same check is made for GHGs (Fig. 2), and the fast-feedback climate sensitivity of  $3^\circ\text{C}$  for doubled  $\text{CO}_2$  is confirmed (Fig. 1).

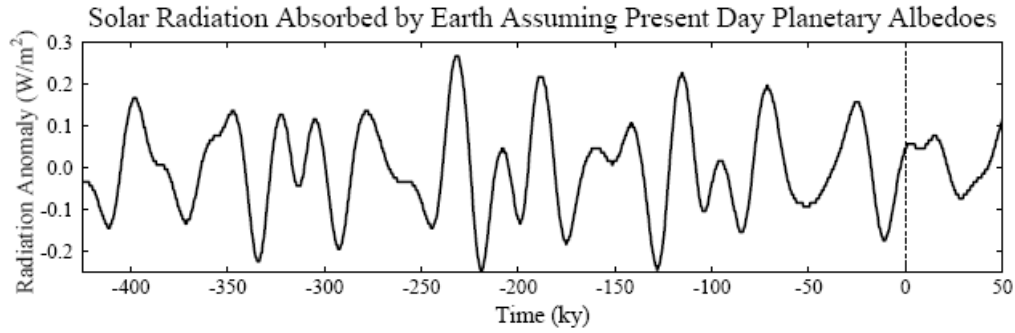


**Fig. S2. Annual-mean global-mean perturbation of the amount of solar radiation absorbed by the Earth, calculated by assuming present-day seasonal and geographical distribution of albedo.**

All the problems associated with imprecise knowledge of aerosol properties become moot if, as is appropriate, aerosols are included in the fast feedback category. Indeed, soil dust, sea salt, dimethylsulfide, and other aerosols are expected to vary (in regional, inhomogeneous ways) as climate changes. The effect of these aerosol changes is fully included in the observed global temperature change. The climate sensitivity that we derive in Fig. S1 includes the aerosol effect accurately, because both the climate forcings and the global climate response are known. The indirect effect of aerosol change on clouds is, of course, also included precisely.

**Earth orbital (Milankovitch) climate forcing.** Figure S2 shows the perturbation of solar radiation absorbed by the Earth due to changes in Earth orbital elements, i.e., the tilt of the Earth’s spin axis relative to the orbital plane, the eccentricity of the Earth’s orbit, and the time of year at which the Earth is closest to the sun (precession of equinoxes). This perturbation is calculated assuming fixed (present day) seasonal and geographical distribution of planetary albedo. It measures the global forcing that instigates the glacial-interglacial climate changes.

This weak forcing is negligible, per se, on global-mean annual-mean basis. However, regional seasonal insolation perturbations are as much as several tens of  $W/m^2$ . These insolation perturbations instigate ice sheet and GHG changes, slow feedbacks, which amplify the global annual-mean orbital forcing.

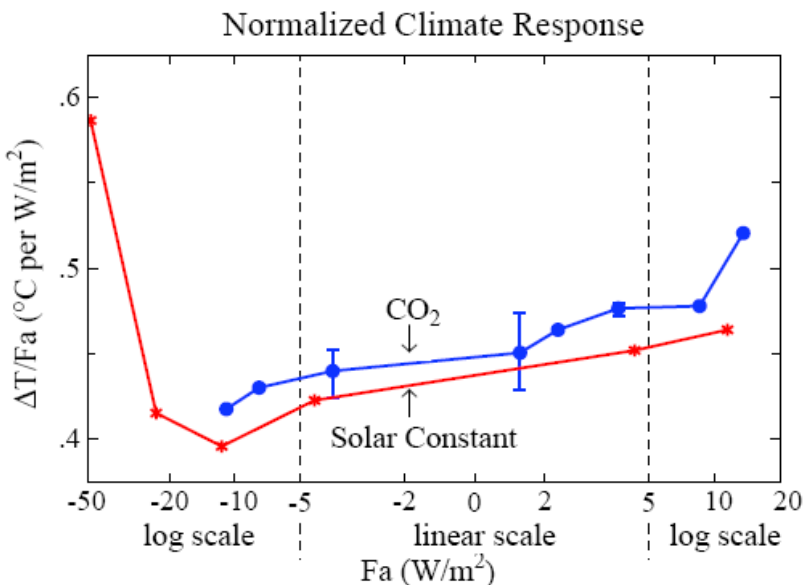


**Fig. S3. Global surface air temperature change (11) after 100 years (mean of years 81-120) in simulations with the Goddard Institute for Space Studies (GISS) modelE (S3, 5) as a function of climate forcing for changes of solar irradiance and atmospheric CO<sub>2</sub>. Fa is the standard adjusted climate forcing (11). Results here are extracted from Fig. 25(a) of (11).**

**Climate response function.** Figure S3 shows that climate forcings of the order of 20-50  $\text{W/m}^2$  are needed to approach either the runaway snowball-Earth feedback or the runaway greenhouse effect, if only the Charney fast feedbacks are included. However, the negative forcing required to approach snowball-Earth is reduced by amplifying slow feedbacks, especially increasing ice sheet area. Indeed, the real-world Earth has experienced snowball conditions (S4), or at least a ‘slushball’ state (S5), on at least two occasions, the most recent ~640 My BP, aided by reduced solar irradiance (41) and favorable continental locations. The mechanism that allowed Earth to escape from the snowball state was probably the reduced weathering in a glaciated world, which allowed volcanic  $\text{CO}_2$  to accumulate in the atmosphere (S4).

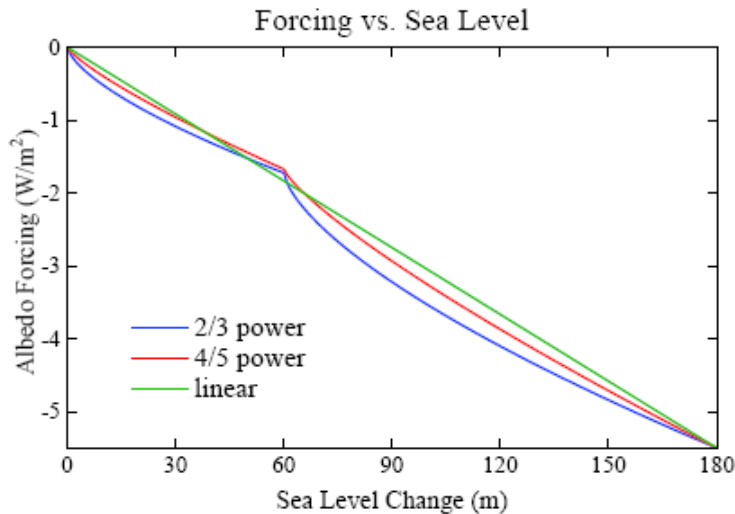
It would, of course, be interesting to extend the simulations of Fig. S3 to both smaller and larger forcings. The reason that the curves in Fig. 2 terminate is that the climate model “bombed” at the next increment of forcing due to failure of one or more of the parameterizations of physical processes in the model when extreme conditions are approached. The accuracy of the representations at extreme temperatures must be improved before the model can be used to simulate well transitions to snowball Earth or the runaway greenhouse effect.

**Ice sheet albedo.** In the present paper we take the surface area covered by an ice sheet to be proportional to the  $4/5$  power of the volume of the ice sheet, based on ice sheet modeling of one of us (VM-D). We extend the formulation all the way to zero ice on the planet, with separate terms for each hemisphere. At 20 ky ago, when the ice sheets were at or near their maximum size in the Cenozoic era, the forcing by the Northern Hemisphere ice sheet was  $-3.5 \text{ W/m}^2$  and the forcing by the Southern Hemisphere ice sheet was  $-2 \text{ W/m}^2$ , relative to the ice-free planet (11). It is assumed that the first 60 m of sea level fall went entirely into growth of the Southern Hemisphere ice sheet. The water from further sea level fall is divided proportionately between hemispheres such that when sea level fall reaches -180 m there is 75 m in the ice sheet of the Southern Hemisphere and 105 m in the Northern Hemisphere.

The climate forcing due to sea level changes in the two hemispheres,  $SL_S$  and  $SL_N$ , is

$$F_{\text{Albedo}} (\text{W/m}^2) = -2 (SL_S/75 \text{ m})^{4/5} - 3.5 (SL_N/105 \text{ m})^{4/5}, \quad (\text{S1})$$

where the climate forcings due to fully glaciated Antarctica ( $-2 \text{ W/m}^2$ ) and Northern Hemisphere glaciation during the last glacial maximum ( $-3.5 \text{ W/m}^2$ ) were derived from global climate model simulations (13).



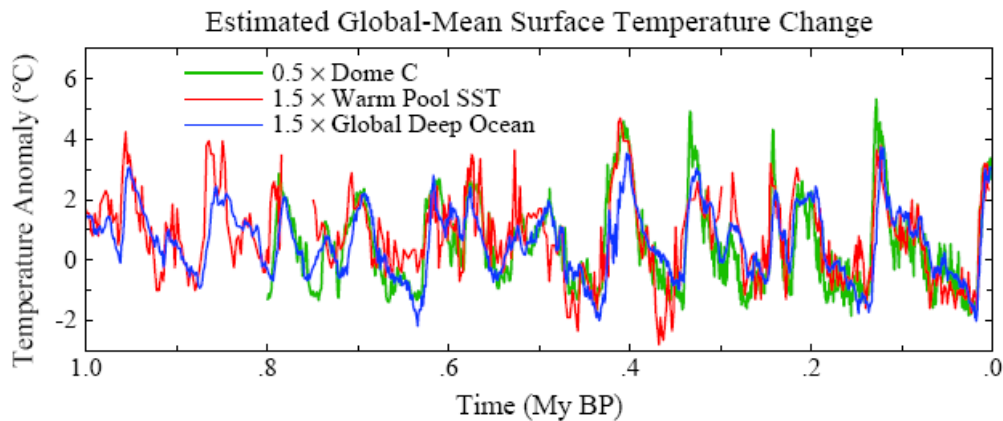
**Fig. S4. Surface albedo climate forcing as a function of sea level for three approximations of the ice sheet area as a function of sea level change, from an ice free planet to the last glacial maximum. For sea level between 0 and 60 m only Antarctica contributes to the albedo change. At the last glacial maximum Antarctica contains 75 m of sea level and the Northern Hemisphere contains 105 m.**

Figure S4 compares results from the present approach with results from the same approach using exponent  $2/3$  rather than  $4/5$ , and with a simple linear relationship between the total forcing and sea level change. Use of exponent  $4/5$  brings the results close to the linear case, suggesting that the simple linear relationship is a reasonably good approximation. The similarity of Fig. 1c in our present paper and Fig. 2c in (7) indicates that change of exponent from  $2/3$  to  $4/5$  did not have a large effect.

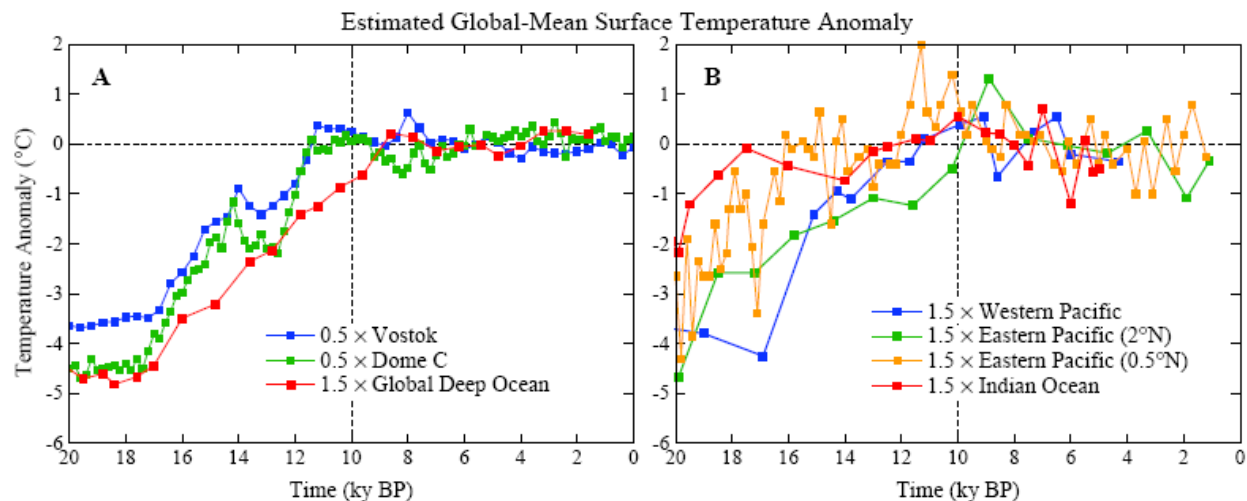
**Global nature of major climate changes.** Climate changes often begin in a specific hemisphere, but the large climate changes are invariably global, in part because of the global GHG feedback. Even without the GHG feedback, forcings that are located predominately in one hemisphere, such as ice sheet changes or human-made aerosols, still evoke a global response (11), albeit with the response being larger in the hemisphere of the forcing. Both the atmosphere and ocean transmit climate response between hemispheres. The deep ocean can carry a temperature change between hemispheres with little loss, but because of the ocean's thermal inertia there can be a hemispheric lag of up to a millennium (see Ocean Response Time, below).

Figure S5 compares temperature change in Antarctica (S6), the tropical sea surface (S7), and the global deep ocean (24). Temperature records are multiplied by specific factors intended to convert the temperature record to an estimate of global temperature change. Based on paleoclimate records, polar temperature change is typically twice the global average temperature change, and tropical temperature change is about two-thirds of the global mean change. This polar amplification of the temperature change is an expected consequence of feedbacks (13), especially the snow-ice albedo feedback. The empirical result that deep ocean temperature changes are only about two-thirds as large as global temperature change is obtained from data for the Pleistocene epoch, when deep ocean temperature change is limited by its approach to the freezing point.

**Holocene climate forcings.** The GHG zero-point for the paleo portion of Fig. 2 is the mean for 10-8 ky BP, a time that should precede any significant anthropogenic effect on GHG amount. It has been suggested that the increase of  $\text{CO}_2$  that began 8000 years ago is due to deforestation and the increase of  $\text{CH}_4$  that began 6000 years ago is caused by rice agriculture (59). Regardless of whether late Holocene  $\text{CO}_2$  and  $\text{CH}_4$  changes are human-made, the GHG forcing is anomalous in that period relative to global temperature change estimated from ocean and ice cores. As



**Fig. S5.** Estimated global temperature change based on measurements at a single point or, in the case of the deep ocean, a near-global stack of ocean drilling sites: Antarctica Dome C (S6), Warm Pool (S7), deep ocean (24).



**Fig. S6. Estimates of global temperature change inferred from Antarctic ice cores (27, S6) and ocean sediment cores (S7-S11), as in Fig. 5 but for a period that allows the Holocene temperature change to be apparent.**

discussed elsewhere (7), the late Holocene is the only time in the ice core record in which the temperature change deviates from that expected due to GHG and surface albedo forcings.

The GHG forcing increase in the second half of the Holocene is  $\sim 3/4 \text{ W/m}^2$ . Such a large forcing, by itself, would create a planetary energy imbalance that could not be sustained for millennia without causing a large global temperature increase, the expected global warming being about  $1^\circ\text{C}$ . Actual global temperature change in this period was small, perhaps a slight cooling. Figure S6 shows estimates of global temperature change obtained by dividing polar temperature change by two or multiplying tropical and deep ocean temperatures by 1.5. Clearly the Earth has not been warming rapidly in the latter half of the Holocene. Thus a substantial (negative) forcing must have been operating along with the positive GHG forcing.

Deforestation causes a negative climate forcing (11), but an order of magnitude too small to balance GHG positive forcing. A much larger negative forcing is expected from human-made aerosols. Aerosol forcing is non-linear, especially the indirect effect on clouds, with aerosols added to a pristine atmosphere being more effective than those added to the current highly polluted atmosphere. Given estimates of a negative forcing of  $1\text{-}2 \text{ W/m}^2$  for today's anthropogenic aerosols (2, 5, 11), a negative aerosol forcing at least of the order of  $0.5 \text{ W/m}^2$  in 1850 is expected. We conclude that aerosols were the predominant negative forcing that opposed the rapid increase of positive GHG forcing in the late Holocene.

The suggestion (59) that GHG increase in the latter half of the Holocene was due to deforestation, fires, and agricultural activities has been criticized on the grounds that the required human-made carbon transfers are unrealistically large (S12). Our present analysis relates to this discussion in several ways.

First, we have shown (Fig. 2) that the paleoclimate global temperature changes are accounted for by the atmospheric and surface albedo ‘forcings’ (which are slow climate feedbacks). Insolation changes due to Earth orbital changes have negligible direct forcing; they operate by instigating surface and atmospheric changes, which are the mechanisms causing global temperature change. The relevance of this observation is that the presumed human-made carbon transfers (59, S12) were based on an assumption that changes of atmospheric  $\text{CO}_2$  and  $\text{CH}_4$  are

proportional to insolation changes, resulting in a presumed requirement of 40 ppm CO<sub>2</sub> and 250 ppb CH<sub>4</sub> of human-made gases. However, CO<sub>2</sub> and CH<sub>4</sub> are accurately determined by global temperature, as shown individually for CO<sub>2</sub> and CH<sub>4</sub> in Figure 6 of (6). Thus the required carbon sources are only the observed increases (~20 ppm CO<sub>2</sub> and 100 ppb CH<sub>4</sub>). In order for humans to be the dominate cause of the Holocene CO<sub>2</sub> increase they need only account for at least 10 ppm of CO<sub>2</sub>, not 40 ppm. Thus carbon isotope analyses (S12) disproving a 40 ppm deforestation source do not contradict the hypothesis that the human impact on atmospheric composition began 6000-8000 years ago.

Second, our GHG-temperature comparison for the period of ice core data (Fig. 2) also show that the anomalous (contrary to flat or slightly decreasing temperature) leap in GHG forcing in the past 6000-8000 years is highly unusual, indeed, unique among the interglacial periods. Thus our analysis supports Ruddiman's (59) hypothesis that significant human effects began several thousand years ago.

Third, our results do not support the contention (59) that human-made forcings averted an ice age. Until the past few decades the net human-made forcing was small and of uncertain sign, as positive GHG and negative aerosol forcings were comparable in magnitude. Today the net human-made forcing is positive and growing rapidly, because CO<sub>2</sub> is continuing to accumulate while global aerosol amounts are stabilizing. Thus the question of when the Earth would have entered the next ice age, if there were no humans on the planet, is rhetorical and of limited interest. Human-made CO<sub>2</sub> will remain in the air for many millennia, eliminating the possibility of another ice age on time scales of interest to humans. Even without CO<sub>2</sub> an ice age could be averted with a small amount of trace gases such as chlorofluorocarbons, so there is no reason that another ice age need occur as long as humans and a technological society remain on the planet. The question instead is whether GHGs can be kept to a level such that climate remains close to conditions of the Holocene, or whether changes are initiated that carry the climate to a very different planetary state, one that is foreign to human experience.

**Ocean response time.** Figure S7 shows the climate response function, defined as the fraction of equilibrium global warming that is obtained as a function of time. This response function was obtained (7) from a 3000-year simulation after instant doubling of atmospheric CO<sub>2</sub>, using GISS modelE (S3, 11) coupled to the Russell ocean model (S13). Note that although 40% of the equilibrium solution is obtained within several years, only 60% is achieved after a century, and

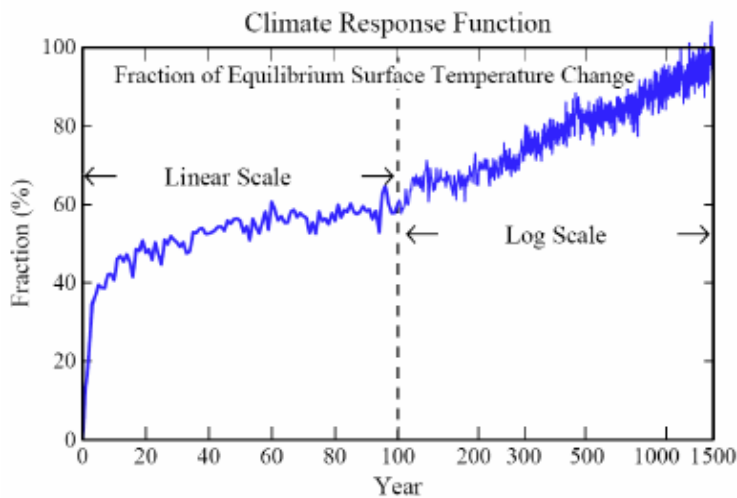


**Fig. S7. Fraction of equilibrium surface temperature response versus time in the GISS climate model (7, 11, S3) with the Russell (S13) ocean. The forcing was doubled atmospheric CO<sub>2</sub>. The ice sheets, vegetation distribution and other long-lived GHGs were fixed.**

nearly full response requires a millennium. The long response time is caused by slow uptake of heat by the deep ocean, which occurs primarily in the Southern Ocean.

This delay of the surface temperature response to a forcing, caused by ocean thermal inertia, is a strong (quadratic) function of climate sensitivity and it depends on the rate of mixing of water into the deep ocean (29). The ocean model used for Fig. S7 may mix somewhat too rapidly in the waters around Antarctica, as judged by transient tracers (S13), reducing the simulated surface response on the century time scale. However, this uncertainty does not qualitatively alter the shape of the response function (Fig. S7).

When the climate model used to produce Fig. S7 is driven by observed changes of GHGs and other forcings it yields good agreement with observed global temperature and ocean heat storage (5). The model has climate sensitivity  $\sim 3^\circ\text{C}$  for doubled  $\text{CO}_2$ , in good agreement with the fast-feedback sensitivity inferred from paleoclimate data.

**Separation of  $\delta^{18}\text{O}$  into ice volume and temperature.**  $\delta^{18}\text{O}$  of benthic (deep ocean dwelling) foraminifera is affected by both deep ocean temperature and continental ice volume. Between 34 My and the last ice age (20 ky) the change of  $\delta^{18}\text{O}$  was  $\sim 3$ , with  $T_{\text{do}}$  change  $\sim 6^\circ\text{C}$  (from  $+5$  to  $-1^\circ\text{C}$ ) and ice volume change  $\sim 180$  msl (meters of sea level). Based on the rate of change of  $\delta^{18}\text{O}$  with deep ocean temperature in the prior period without land ice,  $\sim 1.5$  of  $\delta^{18}\text{O}$  is associated with the  $T_{\text{do}}$  change of  $\sim 6^\circ\text{C}$ , and we assign the remaining  $\delta^{18}\text{O}$  change to ice volume linearly at the rate 60 msl per mil  $\delta^{18}\text{O}$  change (thus 180 msl for  $\delta^{18}\text{O}$  between 1.75 and 4.75).

Thus we assume that ice sheets were absent when  $\delta^{18}\text{O} < 1.75$  with sea level 75 msl higher than today. Sea level at smaller values of  $\delta^{18}\text{O}$  is given by

$$\text{SL (m)} = 75 - 60 \times (\delta^{18}\text{O} - 1.75). \quad (\text{S2})$$

Figure S8 shows that the division of  $\delta^{18}\text{O}$  equally into sea level change and deep ocean temperature captures well the magnitude of the major glacial to interglacial changes.

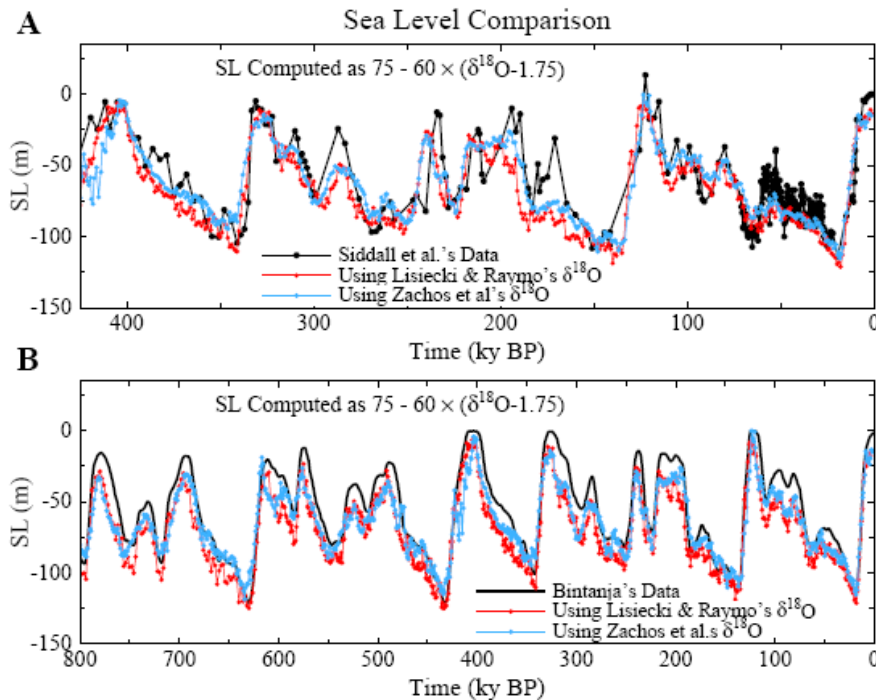


**Fig. S8. (A)** Comparison of Siddall *et al.* (17) sea level record with sea level computed from  $\delta^{18}\text{O}$  via Eq. S2 using two alternative global benthic stacks (24, S14). **(B)** Comparison of Bintanja *et al.* (S15) sea level reconstruction with the same global benthic stacks as in (A).

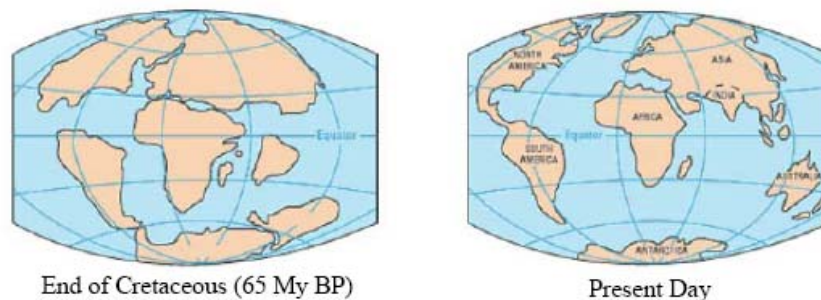


**Fig. S9. Continental locations at the beginning and end of the Cenozoic era (S16).**

**Continental drift and atmospheric CO<sub>2</sub>.** At the beginning of the Cenozoic era 65 My ago the continents were already close to their present latitudes, so the effect of changing continental location per se did not have a large effect on the planet's energy balance (Fig. S9). However, continental drift has a major effect on the balance, or imbalance, of uptake and outgassing of CO<sub>2</sub> by the solid Earth. Outgassing, which occurs in regions of volcanic activity, depends upon the rate at which carbonate-rich oceanic crust is subducted beneath moving continental plates (45). Drawdown of atmospheric CO<sub>2</sub> occurs with weathering of rocks exposed by uplift, with the weathering products carried by rivers to the ocean and eventually deposited as carbonates on the ocean floor (46).

At the beginning of the Cenozoic the African plate was already in collision with Eurasia, pushing up the Alps. India was still south of the equator, but moving north rapidly through a region with fresh carbonate deposits. It is likely that subduction of carbonate rich crust of the Tethys Ocean, long a depocenter for sediments, caused an increase of atmospheric CO<sub>2</sub> and the early Cenozoic warming that peaked ~50 My ago. The period of rapid subduction terminated with the collision of India with Eurasia, whereupon uplift of the Himalayas and the Tibetan Plateau greatly increased weathering rates and drawdown of atmospheric CO<sub>2</sub> (49).

Since 50 My ago the major rivers of the world have emptied into the Indian and Atlantic Oceans. But there is little subduction of oceanic crust associated with the ocean basins in which these sediments are accumulating (45). Thus the present continental geography is the presumed cause of CO<sub>2</sub> drawdown and cooling over the past 50 My.

**Proxy CO<sub>2</sub> data.** Strengths and weaknesses of the four paleo-CO<sub>2</sub> reconstruction methods reported in Fig S10, discussed in detail elsewhere (S17), constrain their utility for rigorously evaluating the CO<sub>2</sub> predictions. In brief, the paleosol method is based on the  $\delta^{13}\text{C}$  of pedogenic carbonate nodules, whose formation can be represented by a two end-member mixing model between atmospheric CO<sub>2</sub> and soil-derived carbon (S18). Variables that need to be constrained or assumed include an estimation of nodule depth from the surface of the original soil, the respiration rate of the ecosystem that inhabits the soil, the porosity/diffusivity of the original soil, and the isotopic composition of the vegetation contribution of respired CO<sub>2</sub>. The uncertainties in CO<sub>2</sub> estimates with this proxy are substantial at high CO<sub>2</sub> ( $\pm 500$ -1000 ppm when CO<sub>2</sub> > 1000 ppm) and somewhat less in the lower CO<sub>2</sub> range ( $\pm 400$ -500 ppm when CO<sub>2</sub> < 1000 ppm).

The stomatal method is based on the genetically-controlled relationship (S19) between the proportion of leaf surface cells that are stomata and atmospheric CO<sub>2</sub> concentrations (S20). The error terms with this method are comparatively small at low CO<sub>2</sub> (<  $\pm 50$  ppm), but the method rapidly loses sensitivity at high CO<sub>2</sub> (> 500-1000 ppm). Because stomatal-CO<sub>2</sub> relationships are often species-specific, only extant taxa with long fossil records can be used (S21). Also, because the fundamental response of stomata is to the partial pressure of CO<sub>2</sub> (S22), constraints on

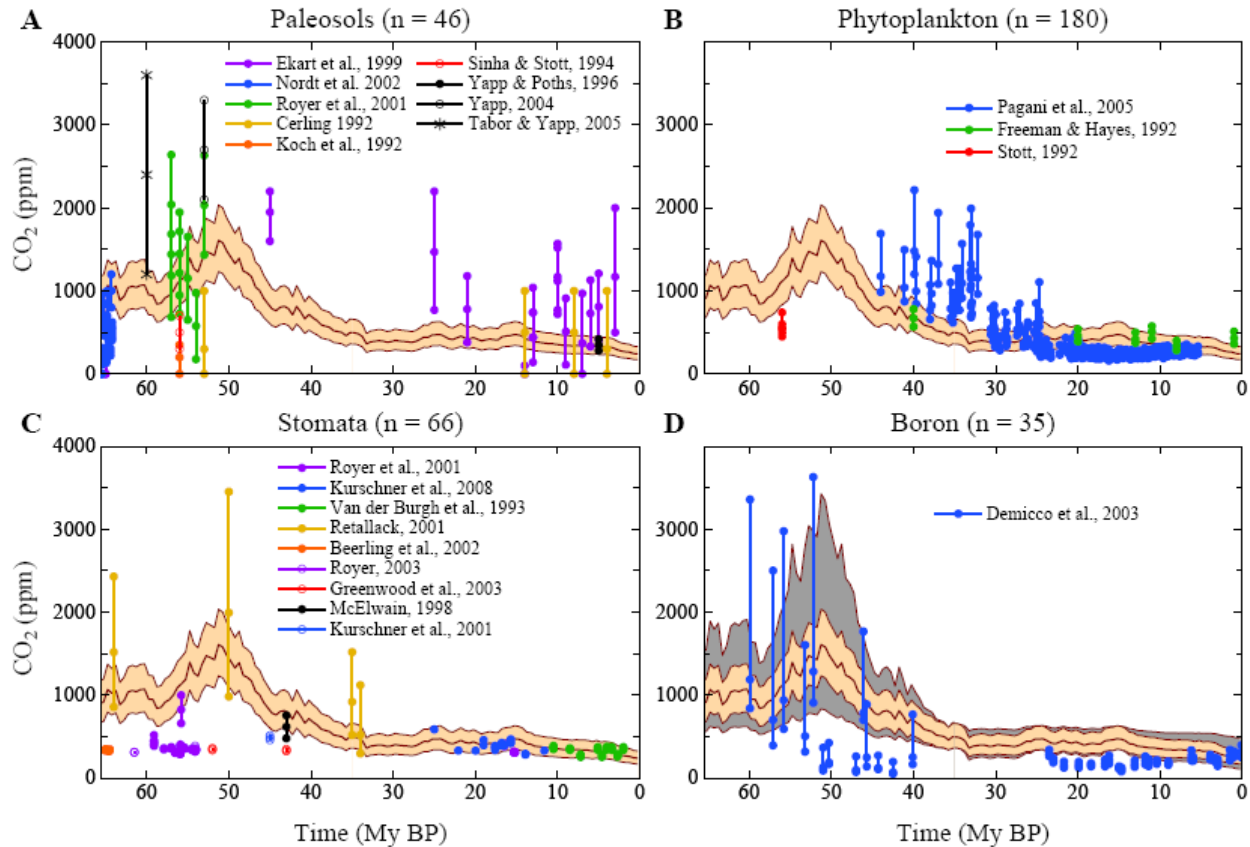


**Fig. S10. Comparison of proxy CO<sub>2</sub> measurements with CO<sub>2</sub> predictions based on deep-ocean temperature, the latter inferred from benthic  $\delta^{18}\text{O}$ . The beige range of model results, intended only to guide the eye in comparing different proxies, is for the case  $T_s = T_{do}$ , the dark central line for the case  $\text{CO}_2 = 450$  ppm at 34 My ago and the borders of the beige area being 325 and 600 ppm. Part D shows the additional range in the model prediction for a 50% uncertainty in the relationship of  $T_s$  and  $T_{do}$ . Our assumption that  $\text{CO}_2$  provides 75% of the GHG throughout the Cenozoic adds additional uncertainty to the predicted  $\text{CO}_2$  amount.**

paleoelevation are required.

The phytoplankton method is based on the Rayleigh distillation process of fractionating stable carbon isotopes during photosynthesis (S23). In a high  $\text{CO}_2$  environment, for example, there is a higher diffusion rate of  $\text{CO}_2$  through phytoplankton cell membranes, leading to a larger available intercellular pool of  $\text{CO}_{2[\text{aq}]}$  and more depleted  $\delta^{13}\text{C}$  values in photosynthate. Cellular growth rate and cell size also impact the fractionation of carbon isotopes in phytoplankton and thus fossil studies must take these factors into account (S24). This approach to reconstructing  $\text{CO}_2$  assumes that the diffusional transport of  $\text{CO}_2$  into the cell dominates, and that any portion of carbon actively transported into the cell remains constant with time. Error terms are typically small at low  $\text{CO}_2$  ( $< \pm 50$  ppm) and increase substantially under higher  $\text{CO}_2$  concentrations (S24).

The boron-isotope approach is based on the pH-dependency of the  $\delta^{11}\text{B}$  of marine carbonate (S25). This current method assumes that only borate is incorporated in the carbonate lattice and that the fractionation factor for isotope exchange between boric acid and borate in solution is well-constrained. Additional factors that must be taken into account include test dissolution and size, species-specific physiological effects on carbonate  $\delta^{11}\text{B}$ , and ocean alkalinity (S26-28). As with the stomatal and phytoplankton methods, error terms are comparatively small at low  $\text{CO}_2$

**Table S1. Climate sensitivities inferred semi-empirically from Cenozoic or Phanerozoic climate change.**

Reference	Period	Doubled CO <sub>2</sub> Sensitivity
Royer et al. (53)	0-420 My	~ 2.8°C
Higgins and Schrag (54)	PETM	~4°C
Pagani et al. (55)	PETM	High

(< ±50 ppm) and the method loses sensitivity at higher CO<sub>2</sub> (> 1000 ppm). Uncertainty is unconstrained for extinct foraminiferal species.

**Climate sensitivity comparisons.** Other empirical or semi-empirical derivations of climate sensitivity from paleoclimate data (Table S1) are in reasonable accord with our results, when account is taken of differences in definitions of sensitivity and the periods considered.

Royer et al. (53) use a carbon cycle model, including temperature dependence of weathering rates, to find a best-fit doubled CO<sub>2</sub> sensitivity of 2.8°C based on comparison with Phanerozoic CO<sub>2</sub> proxy amounts. Best-fit in their comparison of model and proxy CO<sub>2</sub> data is dominated by the times of large CO<sub>2</sub> in the Phanerozoic, when ice sheets would be absent, not by the times of small CO<sub>2</sub> in the late Cenozoic. Their inferred sensitivity is consistent with our inference of ~3°C for doubled CO<sub>2</sub> at times of little or no ice on the planet.

Higgins and Schrag (54) infer climate sensitivity of ~4°C for doubled CO<sub>2</sub> from the temperature change during the Paleocene-Eocene Thermal Maximum (PETM) ~55 My ago Fig.

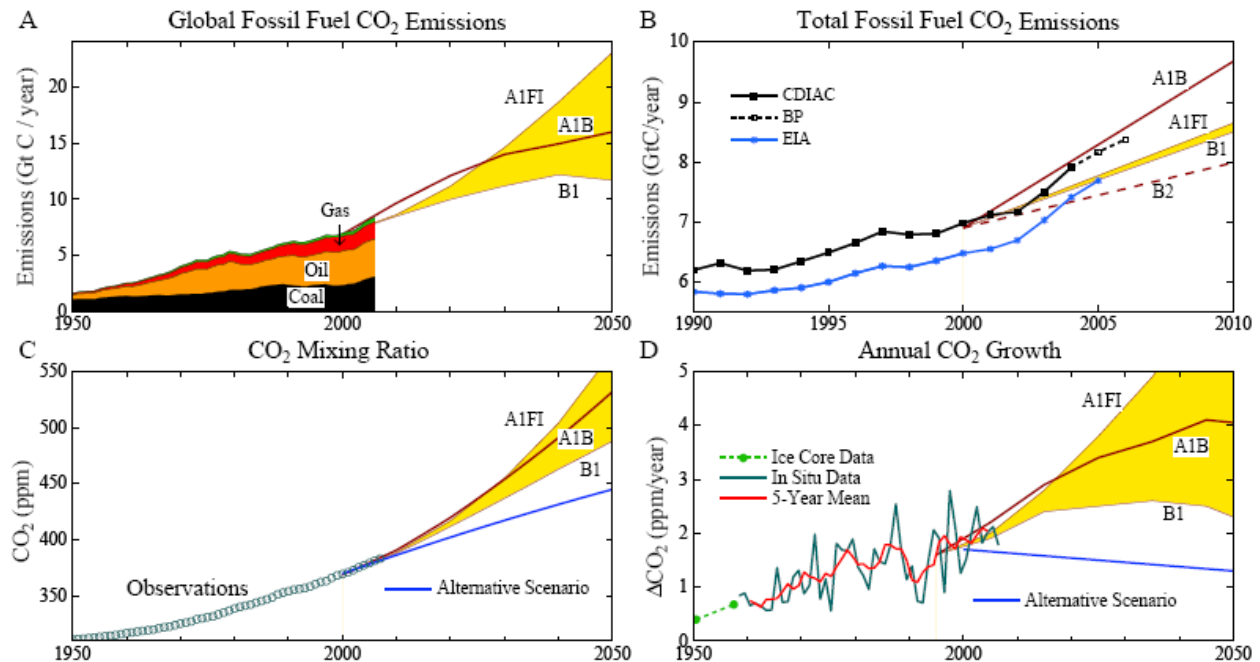


**Fig. S11. (A)** Fossil fuel CO<sub>2</sub> emissions by fuel type (S29, S30), the thin green sliver being gas flaring plus cement production, and IPCC fossil fuel emissions scenarios, **(B)** expansion global emissions to show recent changes more precisely, the EIA values excluding CO<sub>2</sub> emissions from cement manufacture, **(C)** observed atmospheric CO<sub>2</sub> amount and IPCC and “alternative” scenarios for the future, **(D)** annual atmospheric CO<sub>2</sub> growth rates. Data here is an update of data sources defined in (6). The yellow area is bounded by scenarios that are most extreme in the second half of the 21<sup>st</sup> century; other scenarios fall outside this range in the early part of the century.

3), based on the magnitude of the carbon isotope excursion at that time. Their climate sensitivity for an ice-free planet is consistent with ours within uncertainty ranges. Furthermore, recalling that we assume non-CO<sub>2</sub> to provide 25% of the GHG forcing, if one assumes that part of the PETM warming was a direct effect of methane, then their inferred climate sensitivity is in even closer agreement with ours.

Pagani et al. (55) also use the magnitude of the PETM warming and the associated carbon isotopic excursion to discuss implications for climate sensitivity, providing a graphical relationship to help assess alternative assumptions about the origin and magnitude of carbon release. They conclude that the observed PETM warming of about 5°C implies a high climate sensitivity, but with large uncertainty due to imprecise knowledge of the carbon release.

**Greenhouse gas growth rates.** Fossil fuel CO<sub>2</sub> emissions have been increasing at a rate close to the highest IPCC (S31) scenario (Fig. S11B). Increase of CO<sub>2</sub> in the air, however, appears to be in the middle of the IPCC scenarios (Fig. S11C, D), but as yet the scenarios are too close and interannual variability too large, for assessment. CO<sub>2</sub> growth is well above the “alternative scenario”, which was defined with the objective of keeping added GHG forcing in the 21<sup>st</sup> century at about 1.5 W/m<sup>2</sup> and 21<sup>st</sup> century global warming less than 1°C (18).

Non-CO<sub>2</sub> greenhouse gases are increasing more slowly than in IPCC scenarios, overall at approximately the rate of the “alternative scenario”, based on a review of data through the end of 2007 (67). There is potential to reduce non-CO<sub>2</sub> forcings below the alternative scenario (67).

**Fossil fuel and land-use CO<sub>2</sub> emissions.** Figure S12 shows estimates of anthropogenic CO<sub>2</sub> emissions to the atmosphere. Although fossil emissions through 2006 are known with good accuracy, probably better than 10%, reserves and potential reserve growth are highly uncertain. IPCC (S31) estimates for oil and gas proven reserves are probably a lower limit for future oil and

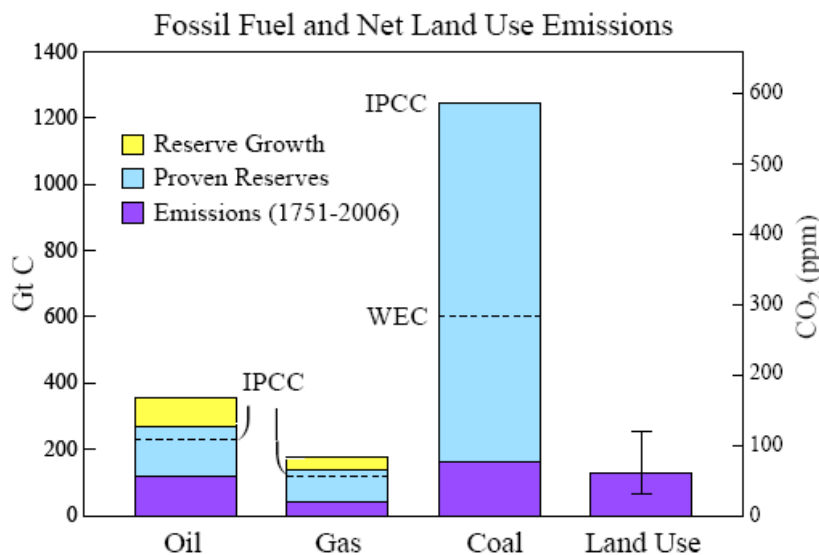


**Fig. S12. Fossil fuel and land-use CO<sub>2</sub> emissions, and potential fossil fuel emissions.** Historical fossil fuel emissions are from the Carbon Dioxide Information Analysis Center (CDIAC, S29) and British Petroleum (BP, S30). Lower limits on oil and gas reserves are from IPCC (S31) and higher limits are from the United States Energy Information Administration (EIA, 78). Lower limit for coal reserves is from the World Energy Council (WEC, S32) and upper limit from IPCC (S31). Land use estimate is from integrated emissions of Houghton/2 (Fig. S14) supplemented to include pre-1850 and post-2000 emissions; uncertainty bar is subjective.

gas emissions, but they are perhaps a feasible goal that could be achieved via a substantial growing carbon price that discourages fossil fuel exploration in extreme environments together with national and international policies that accelerate transition to carbon-free energy sources and limit fossil fuel extraction in extreme environments and on government controlled property.

Coal reserves are highly uncertain, but the reserves are surely enough to take atmospheric CO<sub>2</sub> amount far into the region that we assess as being “dangerous”. Thus we only consider scenarios in which coal use is phased out as rapidly as possible, except for uses in which the CO<sub>2</sub> is captured and stored so that it cannot escape to the atmosphere. Thus the magnitude of coal reserves does not appreciably affect our simulations of future atmospheric CO<sub>2</sub> amount.

Integrated 1850-2008 net land-use emissions based on the full Houghton (81) historical emissions (fig. S14), extended with constant emissions for the past several years, are 79 ppm CO<sub>2</sub>. Although this could be an overestimate by up to a factor of two (see below), substantial pre-1850 deforestation must be added in. Our subjective estimate of uncertainty in the total land-use CO<sub>2</sub> emission is a factor of two.

**The modern carbon cycle.** Atmospheric CO<sub>2</sub> amount is affected significantly not only by fossil fuel emissions, but also by agricultural and forestry practices. Quantification of the role of land-use in the uptake and release of CO<sub>2</sub> is needed to assess strategies to minimize human-made climate effects.

Figure S13 shows the CO<sub>2</sub> airborne fraction, AF, the annual increase of atmospheric CO<sub>2</sub> divided by annual fossil fuel CO<sub>2</sub> emissions. AF is a critical metric of the modern carbon cycle, because it is based on the two numbers characterizing the global carbon cycle that are well known. AF averages 56% over the period of accurate data, which began with the CO<sub>2</sub> measurements of Keeling in 1957, with no discernable trend. The fact that 44% of fossil fuel emissions seemingly “disappears” immediately provides a hint of optimism with regard to the possibility of stabilizing, or reducing, atmospheric CO<sub>2</sub> amount.

That optimism needs to be tempered, as we will see, by realization of the magnitude of the actions required to halt and reverse CO<sub>2</sub> growth. However, it is equally important to realize that assertions that fossil fuel emissions must be reduced close to 100% on an implausibly fast schedule are not necessarily valid.

A second definition of the airborne fraction, AF2, is also useful. AF2 includes the net anthropogenic land-use emission of CO<sub>2</sub> in the denominator. This AF2 definition of airborne fraction has become common in recent carbon cycle literature. However, AF2 is not an observed or accurately known quantity; it involves estimates of net land-use CO<sub>2</sub> emissions, which vary among investigators by a factor of two or more (2).

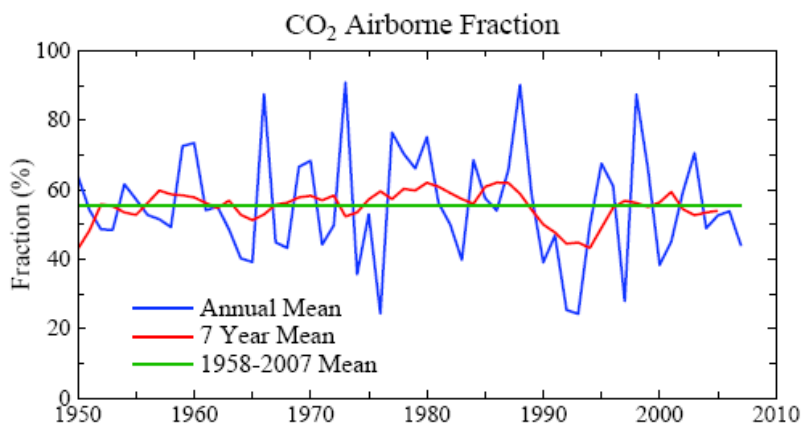


**Fig. S13. CO<sub>2</sub> airborne fraction, AF, the ratio of annual observed atmospheric CO<sub>2</sub> increase to annual fossil fuel CO<sub>2</sub> emissions.**

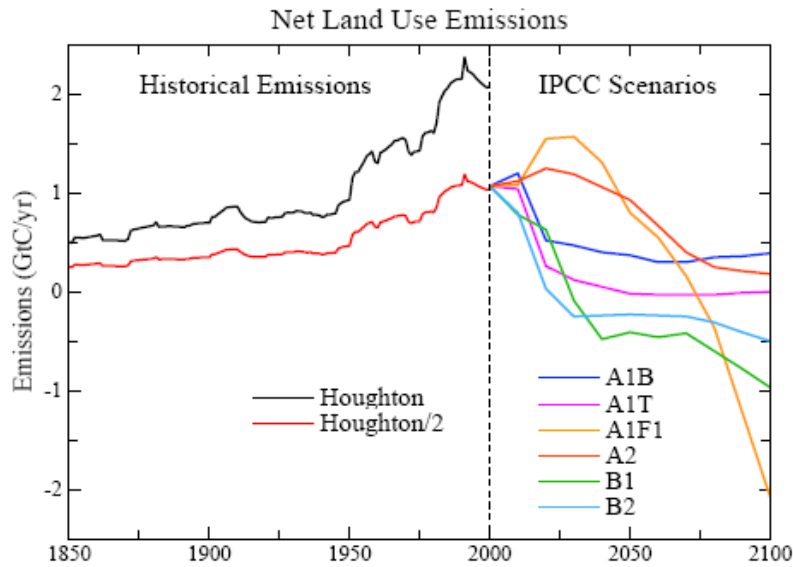


**Fig. S14.** Left side: estimate by Houghton et al. (81) of historical net land-use CO<sub>2</sub> emissions, and a 50 percent reduction of that estimate. Right side: IPCC (2) scenarios for land-use CO<sub>2</sub> emissions.

Figure S14 shows an estimate of net land-use CO<sub>2</sub> emissions commonly used in carbon cycle studies, labeled “Houghton” (81), as well as “Houghton/2”, a 50% reduction of these land-use emissions. An over-estimate of land-use emissions is one possible solution of the long-standing “missing sink” problem that emerges when the full “Houghton” land-use emissions are employed in carbon cycle models (2, S31, 77).

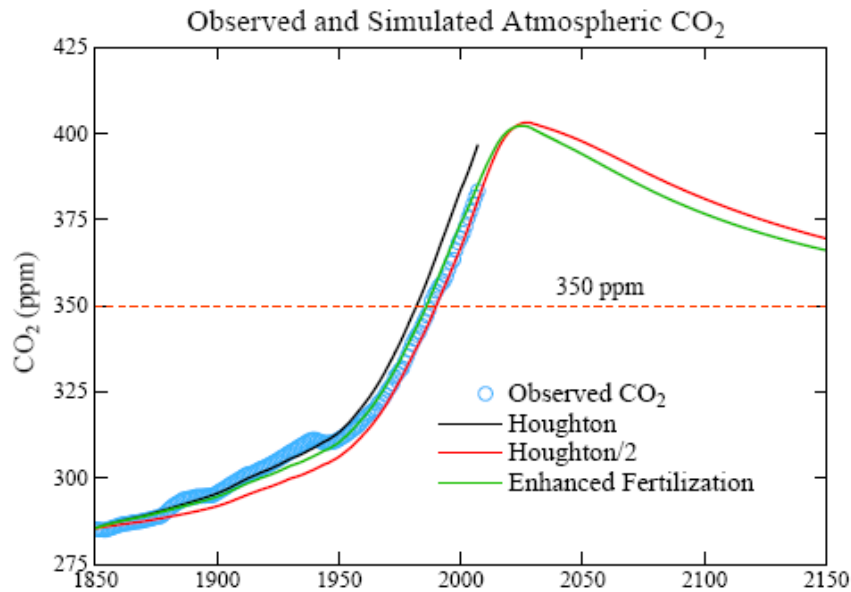


**Fig. S15.** Computed and observed time evolution of atmospheric CO<sub>2</sub>. “Enhanced Fertilization” uses the full “Houghton” land use emissions for 1850–2000. “Houghton/2” and “Enhanced Fertilization” simulations are extended to 2100 assuming coal phase-out by 2030 and the IPCC (2) A1T land-use scenario. Observations are from Law Dome ice core data and flask and in-situ measurements (6, S33, <http://www.esrl.noaa.gov/gmd/ccgg/trends/>).

Principal competing solutions of the “missing sink” paradox are (1) land-use CO<sub>2</sub> emissions are over-estimated by about a factor of two, or (2) the biosphere is being “fertilized” by anthropogenic emissions, via some combination of increasing atmospheric CO<sub>2</sub>, nitrogen deposition, and global warming, to a greater degree than included in typical carbon cycle models. Reality may include contributions from both candidate explanations. There is also a possibility that imprecision in the ocean uptake of CO<sub>2</sub>, or existence of other sinks such as clay formation, could contribute increased CO<sub>2</sub> uptake, but these uncertainties are believed to be small.

Figure S15 shows resulting atmospheric CO<sub>2</sub>, and Figure S16 shows AF and AF2, for two extreme assumptions: “Houghton/2” and “Enhanced Fertilization”, as computed with a dynamic-sink pulse response function (PRF) representation of the Bern carbon cycle model (76, 77). Fertilization is implemented via a parameterization (76) that can be adjusted to achieve an improved match between observed and simulated CO<sub>2</sub> amount. In the “Houghton/2” simulation the original value (76) of the fertilization parameter is employed while in the “Enhanced Fertilization” simulation the full Houghton emissions are used with a larger fertilization parameter. Both “Houghton/2” and “Enhanced Fertilization” yield good agreement with the observed CO<sub>2</sub> history, but Houghton/2 does a better job of matching the time dependence of observed AF.

It would be possible to match observed CO<sub>2</sub> to an arbitrary precision if we allowed the adjustment to “Houghton” land-use to vary with time, but there is little point or need for that. Fig. S15 shows that projections of future CO<sub>2</sub> do not differ much even for the extremes of Houghton/2 and Enhanced Fertilization. Thus in Figure 6 we show results for only the case Houghton/2, which is in better agreement with the airborne fraction and also is continuous with IPCC scenarios for land use.

**Implications of Figure 6: CO<sub>2</sub> Emissions and Atmospheric Concentration with Coal Phase-out by 2030.** Figure 6 provides an indication of the magnitude of actions that are needed to return atmospheric CO<sub>2</sub> to a level of 350 ppm or lower. Figure 6 allows for the fact that there is disagreement about the magnitude of fossil fuel reserves, and that the magnitude of useable reserves depends upon policies.

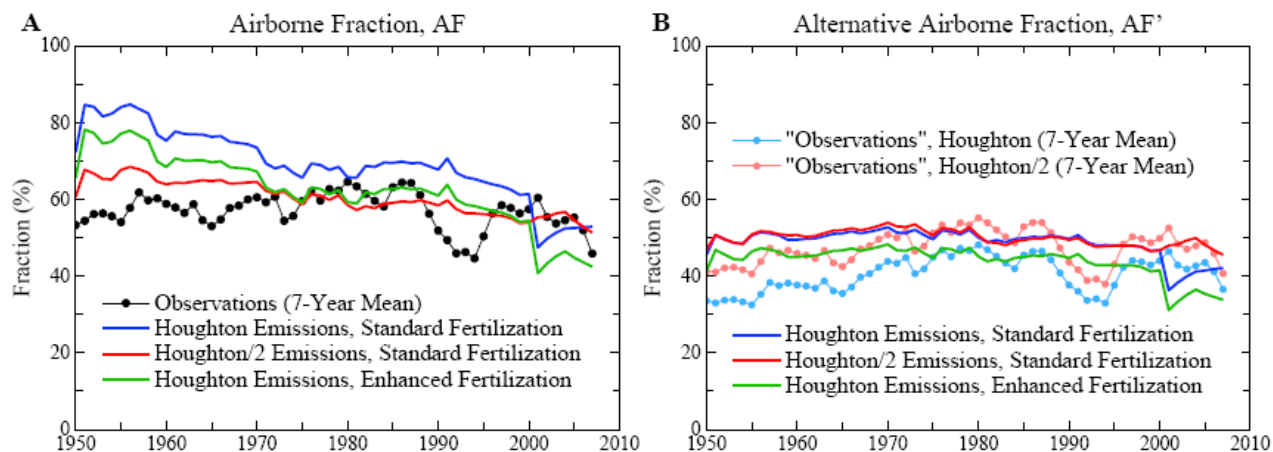


**Fig. S16. (A) Observed and simulated airborne fraction (AF), the ratio of annual CO<sub>2</sub> increase in the air over annual fossil fuel CO<sub>2</sub> emissions, (B) AF2 includes the sum of land use and fossil fuel emissions in the denominator in defining airborne fraction; thus AF2 is not accurately known because of the large uncertainty in land use emissions.**

A basic assumption underlying Figure 6 is that, within the next several years, there will be a moratorium on construction of coal-fired power plants that do not capture and store CO<sub>2</sub>, and that CO<sub>2</sub> emissions from existing power plants will be phased out by 2030. This coal emissions phase out is the sine qua non for stabilizing and reducing atmospheric CO<sub>2</sub>. If the sine qua non of coal emissions phase-out is achieved, atmospheric CO<sub>2</sub> can be kept to a peak amount ~400-425 ppm, depending upon the magnitude of oil and gas reserves.

Figure 6 illustrates two widely different assumptions about the magnitude of oil and gas reserves (illustrated in fig. S12). The smaller oil and gas reserves, those labeled “IPCC”, are realistic if “peak oil” advocates are more-or-less right, i.e., if the world has already exploited about half of readily accessible oil and gas deposits, so that production of oil and gas will begin to decline within the next several years.

There are also “resource optimists” who dispute the “peakists”, arguing that there is much more oil (and gas) to be found. It is possible that both the “peakists” and “resource optimists” are right, it being a matter of how hard we work to extract maximum fossil fuel resources. From the standpoint of controlling human-made climate change, it does not matter much which of these parties is closer to the truth.

Figure 6 shows that, if peak CO<sub>2</sub> is to be kept close to 400 ppm, the oil and gas reserves actually exploited need to be close to the “IPCC” reserve values. In other words, if we phase out coal emissions we can use remaining oil and gas amounts equal to those which have already been used, and still keep peak CO<sub>2</sub> at about 400 ppm. Such a limit is probably necessary if we are to retain the possibility of a drawdown of CO<sub>2</sub> beneath the 350 ppm level by methods that are more-or-less “natural”. If, on the other hand, reserve growth of the magnitude that EIA estimates (Figs. 6 and S12) occurs, and if these reserves are burned with the CO<sub>2</sub> emitted to the atmosphere, then the forest and soil sequestration that we discuss would be inadequate to achieve drawdown below the 350 ppm level in less than several centuries.

Even if the greater resources estimated by EIA are potentially available, it does not mean that the world necessarily must follow the course implied by EIA estimates for reserve growth. If a sufficient price is applied to carbon emissions it will discourage extraction of fossil fuels in the most extreme environments. Other actions that would help keep effective reserves close to the IPCC estimates would include prohibition of drilling in environmentally sensitive areas, including the Arctic and Antarctic.

National policies, in most countries, have generally pushed to expand fossil fuel reserves as much as possible. This might partially account for the fact that energy information agencies, such as the EIA in the United States, which are government agencies, tend to forecast strong growth of fossil fuel reserves. On the other hand, state, local, and citizen organizations can influence imposition of limits on fossil fuel extraction, so there is no guarantee that fossil resources will be fully exploited. Once the successors to fossil energy begin to take hold, there may be a shifting away from fossil fuels that leaves some of the resources in the ground. Thus a scenario with oil and gas emissions similar to that for IPCC reserves may be plausible.

Assumptions yielding the Forestry & Soil wedge in Figure 6B are as follows. It is assumed that current net deforestation will decline linearly to zero between 2010 and 2015. It is assumed that uptake of carbon via reforestation will increase linearly until 2030, by which time reforestation will achieve a maximum potential sequestration rate of 1.6 GtC per year (S34). Waste-derived biochar application will be phased in linearly over the period 2010-2020, by which time it will reach a maximum uptake rate of 0.16 GtC/yr (83). Thus after 2030 there will be an annual uptake of  $1.6 + 0.16 = 1.76$  GtC per year, based on the two processes described.

Thus Figure 6 shows that the combination of (1) moratorium and phase-out of coal emissions by 2030, (2) policies that effectively keep fossil fuel reserves from significantly exceeding the IPCC reserve estimates, and (3) major programs to achieve carbon sequestration in forests and soil, can together return atmospheric CO<sub>2</sub> below the 350 ppm level before the end of the century.

The final wedge in Figure 6 is designed to provide an indication of the degree of actions that would be required to bring atmospheric CO<sub>2</sub> back to the level of 350 ppm by a time close to the middle of this century, rather than the end of the century. This case also provides an indication of how difficult it would be to compensate for excessive coal emissions, if the world should fail to achieve a moratorium and phase-out of coal as assumed as our “sine qua non”.

Assumptions yielding the Oil-Gas-Biofuels wedge in Figure 6B are as follows: energy efficiency, conservation, carbon pricing, renewable energies, nuclear power and other carbon-free energy sources, and government standards and regulations will lead to decline of oil and gas emissions at 4% per year beginning when 50% of the estimated resource (oil or gas) has been exploited, rather than the 2% per year baseline decline rate (77). Also capture of CO<sub>2</sub> at gas-fired power plants will be phased in over the period 2010-2020, and beyond 2020 gas-fired power plants (with CO<sub>2</sub> capture) will use 50% of remaining gas supplies. Also a linear phase-in of liquid biofuels is assumed between 2015 and 2025 leading to a maximum global bioenergy from “low-input/high-diversity” biofuels of ~23 EJ/yr, inferred from Tilman et al. (85), that is used as a substitute for oil; this is equivalent to ~0.5 GtC/yr, based on energy conversion of 50 EJ/GtC for oil. Finally, from 2025 onward, twice this number (i.e., 1 GtC/yr) is subtracted from annual oil emissions, assuming root/soil carbon sequestration via this biofuel-for-oil substitution is at least as substantial as in Tilman et al. (85). An additional option that could contribute to this wedge is using biofuels in powerplants with CO<sub>2</sub> capture and sequestration (84).

**EPICA 800 ky data.** Antarctic Dome C ice core data acquired by EPICA (European Project for Ice Coring in Antarctica) provide a record of atmospheric composition and temperature spanning 800 ky (S6), almost double the time covered by the Vostok data (16) of Figs. 1 and 2. This extended record allows us to examine the relationship of climate forcing mechanisms and temperature change over a period that includes a substantial change in the nature of glacial-interglacial climate swings. During the first half of the EPICA record, the period 800-400 ky BP, the climate swings were smaller, sea level did not rise as high as the present level, and the GHGs did not increase to amounts as high as those of recent interglacial periods.

Figure S17 shows that the temperature change calculated exactly as described for the Vostok data of Fig. 1, i.e., multiplying the fast-feedback climate sensitivity  $\frac{3}{4}^{\circ}\text{C}$  per  $\text{W}/\text{m}^2$  by the sum of the GHG and surface albedo forcings (Fig. S17B), yields a remarkably close fit in the first half of the Dome C record to one-half of the temperature inferred from the isotopic composition of the ice. In the more recent half of the record slightly larger than  $\frac{3}{4}^{\circ}\text{C}$  per  $\text{W}/\text{m}^2$  would yield a noticeably better fit to the observed Dome C temperature divided by two (Figure S18). However, there is no good reason to change our approximate estimate of  $\frac{3}{4}^{\circ}\text{C}$  per  $\text{W}/\text{m}^2$ , because the assumed polar amplification by a factor of two is only approximate.

The sharper spikes in recent observed interglacial temperature, relative to the calculated temperature, must be in part an artifact of differing temporal resolutions. Temperature is inferred from the isotopic composition of the ice, being a function of the temperature at which the snowflakes formed, and thus inherently has a very high temporal resolution. GHG amounts, in contrast, are smoothed over a few ky by mixing of air in the snow that occurs up until the snow is deep enough for the snow to be compressed into ice. In the central Antarctic, where both Vostok and Dome C are located, bubble closure requires a few thousand years (16).

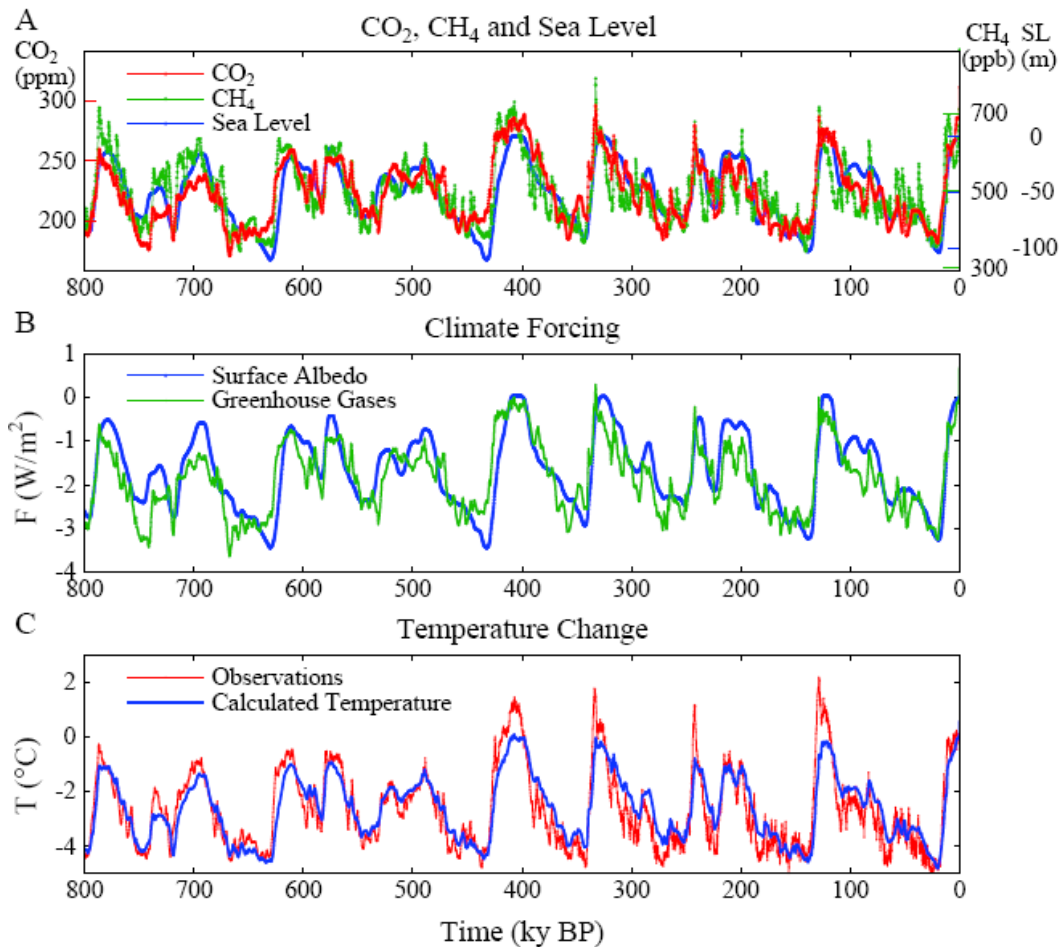


**Fig. S17. (A)** CO<sub>2</sub> (S34), CH<sub>4</sub> (S35) and sea level (S15) for past 800 ky. **(B)** Climate forcings due to changes of GHGs and ice sheet area, the latter inferred from the sea level history of Bintanja et al. (S11). **(C)** Calculated global temperature change based on the above forcings and climate sensitivity  $\frac{3}{4}^{\circ}\text{C per W/m}^2$ . Observations are Antarctic temperature change from the Dome C ice core (S6) divided by two.

Sea level records used to compute the surface albedo forcing in Fig. S17B, generally, are smoothed even more than the GHG forcing. This is in part because the sea level change is inferred from  $\delta^{18}\text{O}$  in ocean sediment cores. The sediments are stirred by bioturbation, resulting in a smoothing of at least several thousand years. In addition, the sea level record used for the albedo forcings in Figs. S17 and S18 (S15) was based in part on an ice sheet model, which was used to separate the ice volume and ocean temperature components of  $\delta^{18}\text{O}$ . The ice sheet model employed did not allow the possibility of rapid ice sheet collapse. Some sea level reconstructions based on evidence of shoreline changes suggest the existence of rapid sea level changes within interglacial periods (30), with the possibility of brief sea level high-stands as much as 9 m above present sea level (31).

**Comparison of Antarctic data sets.** Figure S19 compares Antarctic data sets used in this supplementary section and in our parent paper. This comparison is also relevant to interpretations of the ice core data in prior papers using the original Vostok data.

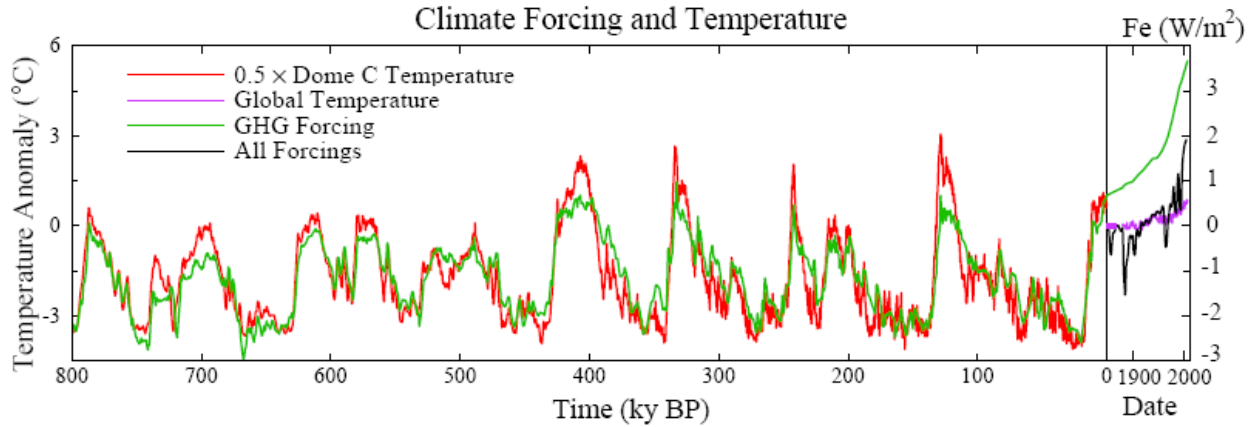


**Fig. S18. Global temperature (left scale) and GHG forcing (right scale) due to CO<sub>2</sub>, CH<sub>4</sub> and N<sub>2</sub>O from Vostok ice core (16, 27). Ratio of temperature and forcing scales is 1.5°C per W/m<sup>2</sup>. Time scale is expanded in the extension to recent years. Modern forcings include human-made aerosols, volcanic aerosols and solar irradiance (5). GHG forcing zero point is the mean for 10-8 ky before present. Net climate forcing and modern temperature zero points are at 1850. The implicit presumption that the positive GHG forcing at 1850 is largely offset by negative human-made forcings (7) is supported by the lack of rapid climate change at that time.**

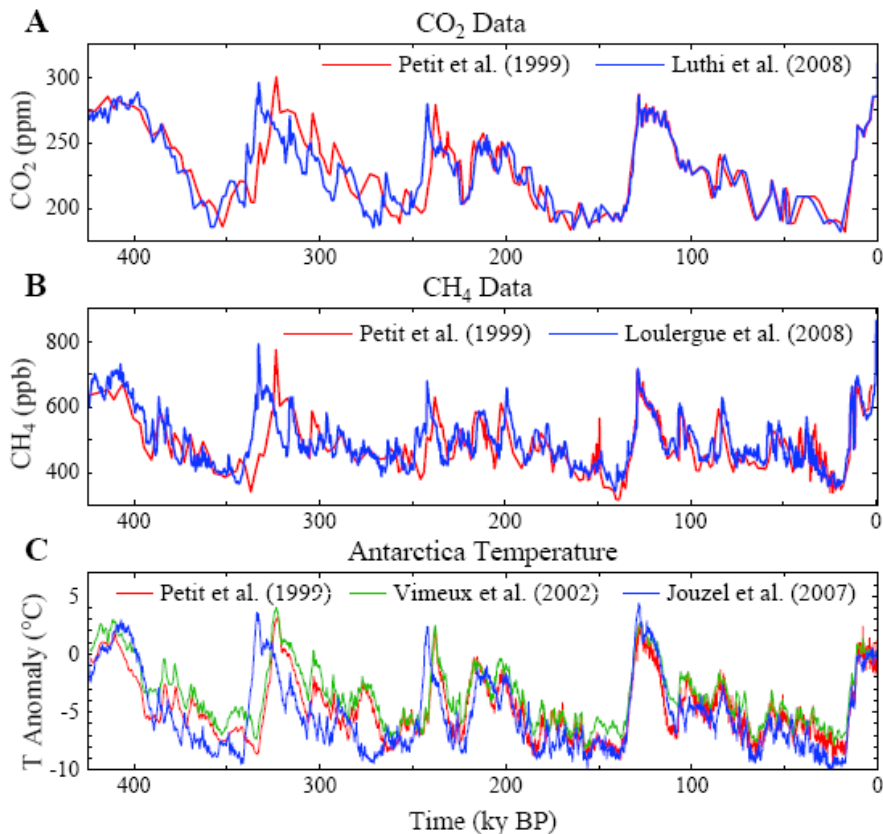


**Fig. S19. Comparison of Antarctic CO<sub>2</sub>, CH<sub>4</sub>, and temperature records in several analyses of Antarctic ice core data.**

The temperature records of Petit et al. (16) and Vimeux et al. (27) are from the same Vostok ice core, but Vimeux et al. (25) have adjusted the temperatures with a procedure designed to correct for climate variations in the water vapor source regions. The isotopic composition of the ice is affected by the climate conditions in the water vapor source region as well as by the temperature in the air above Vostok where the snowflakes formed; thus the adjustment is intended to yield a record that more accurately reflects the air temperature at Vostok. The green temperature curve in Fig. S19C, which includes the adjustment, reduces the amplitude of glacial-interglacial temperature swings from those in the original (red curve) Petit et al. (16) data. Thus it seems likely that there will be some reduction of the amplitude and spikiness of the Dome C temperature record when a similar adjustment is made to the Dome C data set.

The temporal shift of the Dome C temperature data (S6), relative to the Vostok records, is a result of the improved EDC3 (S37, S38) time scale. With this new time scale, which has a  $1\sigma$  uncertainty of  $\sim 3$  ky for times earlier than  $\sim 130$  ky BP, the rapid temperature increases of Termination IV ( $\sim 335$  ky BP) and Termination III ( $\sim 245$  ky BP) are in close agreement with the contention (7) that rapid ice sheet disintegration and global temperature rise should be nearly simultaneous with late spring (April-May-June) insolation maxima at 60N latitude, as was already the case for Terminations II and I, whose timings are not significantly affected by the improved time scale.

The CO<sub>2</sub> data (Fig. S19A) used for Fig. S17 and Fig. S18 are a combined stack of Vostok (16) and Dome C (S39, S36) data on the EDC3 time scale, as presented by Luthi et al. (S35). The addition of Dome C data does not noticeably affect the amplitude of CO<sub>2</sub> glacial-interglacial changes. The CH<sub>4</sub> data (Fig. S19B) used for Figs. S17 and S18 are from the Vostok ice core (S40), but on the EDC3 time scale (S35, S36).

### Supplementary References

- S1. C. Hewitt, J. Mitchell, *Clim. Dyn.* **13**, 834 (1997).
- S2. P. Chylek, U. Lohmann, *Geophys. Res. Lett.* **15**, L04804, doi:10.1029/2007GL032759 (2008).
- S3. G.A. Schmidt *et al.*, *J. Clim.* **19**, 153 (2006).
- S4. P.F. Hoffman, D.P. Schrag, *Terra Nova* **14**, 129 (2002).
- S5. M.A. Chandler, L.E. Sohl, *J. Geophys. Res.* **105**, 20737 (2000).
- S6. J. Jouzel *et al.*, *Science* **317**, 793 (2007).
- S7. M. Medina-Elizade, D.W. Lea, *Science* **310**, 1009 (2005).
- S8. J. Hansen *et al.*, *Proc. Natl. Acad. Sci.* **103**, 14288 (2006).
- S9. D.W. Lea, D.K. Pak, H.J. Spero, *Science*, **289**, 1719 (2000).
- S10. D. W. Lea *et al.*, *Q. Sci. Rev.*, **25**, 1152 (2006).
- S11. R. Saraswat, *et al.*, *Geophys. Res. Lett.*, **32**, L24605 (2005).
- S12. W.S. Broecker, T.F. Stocker, *EOS Trans. AGU* **87**, 27 (2006).
- S13. G.L. Russell, *et al.*, *Dyn. Atmos. Oceans* **9**, 253 (1995).
- S14. L.E. Lisiecki, M.E. Raymo, *Paleocean.* **20**, PA1003 (2005).
- S15. R. Bintanja *et al.*, *Nature* **437**, 125 (2005).
- S16. E.A. Keller, N. Pinter, in *This Dynamic Earth: The Story of Plate Tectonics*, eds. J. Kious, R.I. Tilling, Prentice-Hall, New York, (1996).
- S17. D. L. Royer, R. A. Berner, D. J. Beerling, *Earth-Science Reviews* **54**, 349 (2001).
- S18. T. E. Cerling, *Am. J. Sci.* **291**, 377 (1991).
- S19. J. E. Gray *et al.*, *Nature* **408**, 713 (2000).
- S20. F. I. Woodward, *Nature* **327**, 617 (1987).
- S21. D. L. Royer, *Rev. Palaeobot. Palynol.* **114**, 1 (2001).
- S22. F. I. Woodward, F. A. Bazzaz, *J. Exper. Bot.* **39**, 1771 (1988).

- S23. B. N. Popp, *et al.*, *Amer. J. Sci.* **289**, 436 (1989).
- S24. M. Pagani, *Philosophical Transactions of the Royal Society London A* **360**, 609 (2002).
- S25. A. J. Spivack, *et al.*, *Nature* **363**, 149 (1993).
- S26. D. Blamart *et al.*, *Geochem., Geophys., Geosys.* **8**, Q12001, doi:10.1029/2007GC001686 (2007).
- S27. D. Lemarchand, *et al.*, *Nature* **408**, 951 (2000).
- S28. M. Pagani, *et al.*, *Geochimica et Cosmochimica Acta* **69**, 953 (2005).
- S29. G. Marland, *et al.*, *Trends*, Carbon Dioxide Information Analysis Center, Oak Ridge Nat. Lab., U.S. DOE, Oak Ridge, TN (2006).
- S30. British Petroleum, *Stat. Rev. World Energy*, [www.bp.com/pdf/statistical\\_review\\_of\\_world\\_energy\\_full\\_report2006.pdf](http://www.bp.com/pdf/statistical_review_of_world_energy_full_report2006.pdf) (2006).
- S31. Intergovernmental Panel on Climate Change (IPCC), *Climate Change 2001: Mitigation*, B. Metz *et al.*, Eds. (Cambridge Univ. Press, New York, 2001).
- S32. World Energy Council (2007), *Survey of Energy Resources*, [http://www.worldenergy.org/publications/survey\\_of\\_energy\\_resources\\_2007/default.asp](http://www.worldenergy.org/publications/survey_of_energy_resources_2007/default.asp) (2007).
- S33. C.D. Keeling, T.P. Whorf, *Trends: A Compendium on Global Change*, Carbon Dioxide Information Analysis Center, Oak Ridge Nat. Lab., U.S. DOE, Oak Ridge, TN (2005).
- S34. Intergovernmental Panel on Climate Change (IPCC), *Land Use, Land-Use Change, and Forestry*, R.T. Watson *et al.*, Eds. (Cambridge Univ. Press, Cambridge, UK, 2000).
- S35. D. Luthi *et al.*, *Nature* (in press).
- S36. L. Loulergue, *et al.*, *Nature* (cond. accepted, 2008).
- S37. F. Parrenin, *et al.*, *Clim. Past* **3**, 243 (2007).
- S38. G. Dreyfus *et al.*, *Clim. Past* **3**, 341 (2007).
- S39. U. Siegenthaler, *et al.*, *Science* **310**, 1313 (2005).
- S40. R. Spahni *et al.*, *Science* **310**, 1317 (2005).